ISSN: 2581-4311
DOI: doi.org/10.30967/IJCRSET/Anshebo-Getachew-Alemu/185

URF PUBLISHERS
connect with research world

International Journal of Current Research in Science, Engineering & Technology

https://urfpublishers.com/journal/ijcrset

Vol: 8 & Iss: 2

Research Article

Analysis of Photochemical Kinetics Dependence on Thickness in Dye-Sensitized Nickel Oxide Films with Scanning Electrochemical Microscopy

Anshebo Getachew Alemu*

Department of Physics, Faculty of Natural and Computational Science, Samara University of Applied Science, Ethiopia

---

Citation: Alemu AG. Analysis of Photochemical Kinetics Dependence on Thickness in Dye-Sensitized Nickel Oxide Films with Scanning Electrochemical Microscopy. *Int J Cur Res Sci Eng Tech* 2025; 8(2), 314-321. DOI: doi.org/10.30967/IJCRSET/Anshebo-Getachew-Alemu/185

Received: 16 May, 2025; **Accepted:** 21 May, 2025; **Published:** 23 May, 2025

***Corresponding author:** Anshebo Getachew Alemu, Department of Physics, Faculty of Natural and Computational Science, Samara University of applied Science, Ethiopia, Tel: +251 974413118, Email: getachew2013alemu@yahoo.com

---

ABSTRACT

Scanning electrochemical microscopy (SECM) in feedback mode was used to investigate the photochemical kinetics of dye-sensitized solar cells (DSSCs). In this study, two organic dyes, coumarin (C343) and CW1, were used to sensitize nickel oxide (NiO)-based photo electrochemical cells. Six NiO/C343 films with different thicknesses were the subject of a methodical investigation to look at how they affected the charge transfer kinetics. The absorption cross-section (Φhv), the reduction rate constant (kred) and the effective rate constant (keff) were the three most crucial kinetic parameters that were quantitatively evaluated. The findings unequivocally demonstrate that dye regeneration kinetics demonstrated exceptional sensitivity to incident light intensity, electrode film thickness and sensitizer molecular structure. The fundamentals of the interfacial charge transfer mechanisms that control DSSC performance are explored in this article, which also emphasizes the significance material and operating conditions are to photochemical kinetics. A powerful foundation for spatially resolved analysis of photo electrochemical systems is provided by the SECM-based the approach.

Keywords: Nickel oxide; Kinetic parameters; Scanning electrochemical microscopy

---

Introduction

Since they can be combined with a broad variety of visible-light sensitizers and exhibit good hole-transporting properties, dye-sensitized nickel oxide (NiO) photocathodes have received significant attention to be utilized in p-type dye-sensitized solar cells (p-DSCs), photo electrochemical water splitting and solar fuel generation[1].The NiO film structure and in particular the thickness, which determines light absorption, charge generation and transport kinetics, is still the crucial element in the photochemical efficiency of these systems despite developments in dye structure and interfacial design. Although recent research has proved the influence of film thickness not only on the dye loading capacity but also on the charge collecting efficiency and recombination kinetics, the in-depth understanding of the related effects is still unknown[2].

As new devices require fine control of optical transparency and charge transport in ultrathin geometries, the understanding gap makes it difficult to rationally design high-performance NiO-based devices[3]. Because it has an effect on light harvesting, charge carrier diffusion and interfacial charge transfer simultaneously, film thickness in NiO films is an optimization problem. Thicker films increase optical density and dye adsorption but also form longer hole-transport pathways, which increases the risk of recombination losses[4]. Thin films reduce charges' travel distances but can also be plagued by poor light absorption and increased interfacial recombination at the substrate-electrolyte interface[5].The spatially localized photochemical kinetic processes that govern the overall performance of the device is obscured by conventional characterization methods like electrochemical impedance spectroscopy and current-voltage measurements that are capable of yielding only macroscopic information.The requirement to unscramble the interplay between film microstructure and photochemical kinetics by spatially resolved methods has been brought out by recent work[6].

A incredibly powerful technique for examining photochemical reactions at high spatial and temporal resolution,scanning electrochemical microscopy (SECM) has special strengths in examining thickness-dependent kinetics[7]. Photochemical activity and morphology of the film are coupled by nature as a result of SECM, which allows mass transport processes, recombination dynamics and charge transfer rates to be measured locally at the nanoscale, unlike bulk electrochemical techniques[8]. Two new modes, redox competition and feedback modes, of SECM, introduced in recent years, have been successfully utilized to investigate where the photocurrent generation and spots of recombination occur in dye-sensitized systems[9].SECM is in a good position to investigate how film thickness of NiO affects the competition between charge collection and recombination, a key factor for improving device efficiency.

The influence of the thickness of NiO films (0.5-5µm) on photochemical reaction kinetics in dye-sensitized systems is examined in detail in this work by using sophisticated SECM techniques.The paper reveal thickness effects on interfacial charge transfer, transport of charge and light harvesting by combining high-resolution SECM imaging with transient photocurrent studies and impedance spectroscopy[10]. Our research demonstrates a non monotonic correlation between film thickness and photochemical efficiency indicating an optimum range of film thicknesses that balances light harvesting and minimum recombination losses. With applic ability to p-DSCs, solar fuel generation and other photo electrochemical reactions involving control of charge carrier dynamics with considerable accuracy,these findings provide novel design ideas for NiO-based photoelectrodes[11].

A new photo-electrochemical cell family has been newly emerged: the P-DSSC. The photo-excited sensitizer (HOMO) in p-type DSSC is reductively quenched by injecting holes into the valence band of a p-type semiconductor (p-SC)[12,13]. The excited state dye D* injects a hole into the semiconductor valence band (VB), decreasing the amount of dye D, following the process-based operation mechanism of P-type DSSC.If the charge recombination reaction between the reduced sensitizer and hole in valence band (h+/VB p-SC) is acceptable to the redox mediator (M) at a sufficiently slow rate.

The injected holes diffuse to the TCO at the back side, pass through the external circuit and reach the counter electrode, where they oxidize the redox mediator to its original state[14,15]. Parameters affecting overall performance, stability and conversion efficiency have been the focus of several studies. Efforts were made to prepare P-type nanostructure films, including NiO[16], CuO[17],CuSCN[18], CuGaO[19], CuCrO2[20],and K-doped ZnO[21,22], compared to that provided to n-type DSSC. P-type semi-conductors have been interested in NiO due to its high stability and large band gap (e.g., 3.6 to 4eV).

To avoid charge recombination between the injected electron and the photo oxidi sed dye , dye regeneration is a crucial process that minimises the loss of dye. It is critical that the interfacial kinetic process be critical to the process of a photoelectrochemical cell. Electron recombination with holes in the valence band of p-type oxides and hole injection are critical to regeneration in P-type DSSC. The photovoltaic efficiency and regeneration kinetics of dye-sensitized solar cells can be seriously affected by the film thickness[23,24].To characterize the rate constant of electron transfer at the interface, time-resolved spectroscopy (TRTS) was developed to study the kinetics of electron transfer at dye-sensitized solar cells[25-28].

Besides, scanning electrochemical microscopy has also been shown to be a powerful method to calculate ET kinetics at various interfaces, such as polymer/ liquid interfaces[29], liquid/ liquid interfaces[30] and redox enzymes[31].

According to a recent study by the Prof. G. Wittstock group at the University of Oldenburg in Germany, scanning electrochemical microscopy is a novel method of investigating electron transfer at dye-sensitized semiconductor/electrolyte interfaces **(Figure 1)**. They addressed about the regeneration kinetics of ZnO/D149, ZnO/Eosin and ruthenium (II)-sensitized TiO2 interfaces[32-36].

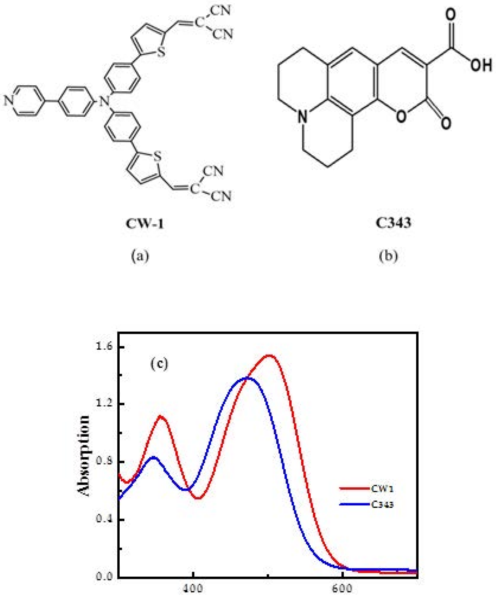

Figure 1: Chemical structure of (a) CW1; (b) C343 dyes; (c) Absorbance of CW1 and C343 dyes

The NiO/C343 films of six distinct thicknesses were investigated in detail in this work. This was accomplished by modifying the dip-coating deposition parameters for NiO and then sensitizing the films in a C343 dye solution for a full night. There are two main analyses in the article: First, the regeneration rates of C343 and CW1 dyes are compared using SECM measurements. Second, a thorough analysis of the kinetic parameters for C343-sensitized NiO films in each of the six thickness ranges that SECM produces. This methodical approach makes it possible to fully understand the kinetics of thickness-dependent charge transfer in the dye regeneration process depicted in **(Figure 1)**.

Materials and Methods

Preparation of the NiO/Dye film

Particles of nickel oxide (NiO) (about 20 nm in size, 99.9%, Informant Advanced Materials) were ball-milled in ethanol with a few acetate droplets. A fine dispersion was achieved by sonicating and stirring the mixture of the aforementioned colloidal solution, ethyl cellulose (Aldrich) and terpinol anhydrous (≥99.5%, Fluka) alternately. The mixture's ethanol was evaporated using a rotary evaporator to create a paste. After being dip coated with a nickel acetate (+98%, Alfa Aesar) ethanol (≥99.7%, Merck) solution (0.05M), FTO glass (Nippon sheet glass, resistance 13 Ω/square) was dried before screen printing[37,38].

SECM apparatus and procedure

A Pt wire counter electrode and a Pt wire quasi-reference electrode were used in the SECM studies. Using an x-y-z stepper motor system, positioning was done. A 5cm Pyrex glass capillary was vacuum-sealed with a Pt wire with a radius of 12.5µm **(Figure 2)**. A wheel with 180-grid carbimet paper disks and 0.3µm micro polishing cloths was used for three minutes to polish and conically shape the UME. Since RG is the ratio of the diameters of the Pt wire and the glass sheath, the UME was sharpened to RG ~ 10. Prior to every experiment, the UME was cleaned with ethanol and water after being polished with 0.3µm powder. A Pt wire was used to short circuit the sensitized NiO electrode to the electrolyte, which was positioned at the bottom of a small volume electrochemical cell.

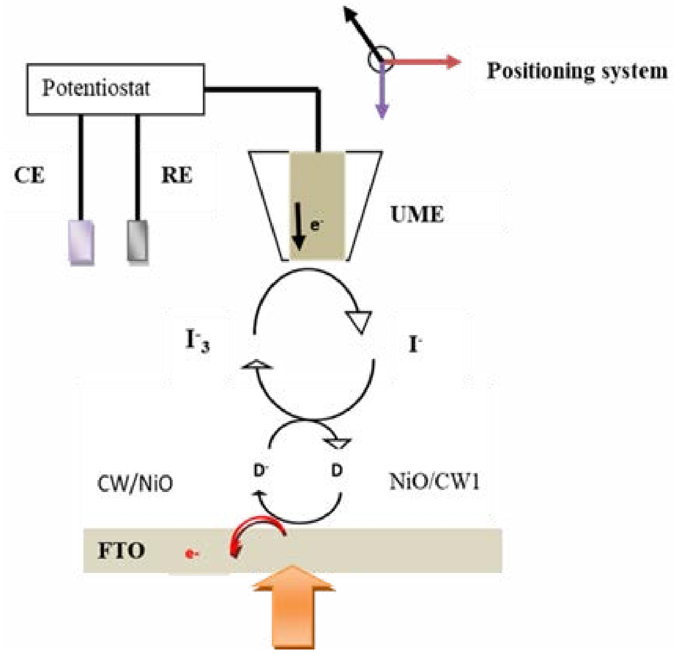

Figure 2: Schematic view of the processes involved in the SECM feedback experiment with dye sensitizedNiO film substrate and I_3^- redox mediators under illumination in short circuit photo electrochemical cell configuration. The structural formula of CW1 is shown in the inset

The LEDs' emission spectra were contrasted with the NiO/C343 and NiO/CW1 films' absorption spectra. An objective lens was utilized to concentrate the LEDs on the dye-sensitized film near the cell, giving the photo-illuminated spot a diameter of approximately 0.0785 cm2[39-42]. Under illumination from red and blue LEDs with systematically varying light intensities, the SECM method curves were used to analyze the photochemical kinetics via electron transfer from the redox electrolyte. **(Figure 2)** illustrates how the LED intensities at the locations of the NiO/C343 and NiO/CW1 samples can be calibrated thanks to the system's integrated light sensor. Nonetheless, the SECM operating principle is explained in[43,44].

The expression of observed power in terms of photon flux density is explained by the math that follows. It summarizes the incident light power (P = 58µJs^{-1} for blue LEDs, P = 56µJs^{-1} for red LEDs) and photon flux (Jhv = 2.9210^{-9} mol s^{-1}cm^{-2} for blue LEDs, Jhv = 3.85×10-9 mol s^{-1}cm^{-2} for red LEDs) from which the number of photons per second is calculated using equation (1a).

$$N_{hv} = \frac{P.\lambda}{h.c} \quad (1)$$

Where h plank constant, h = 6.62606810^{-34} m^{2}kg s^{-1}, C=2.9999910^8 m s^{-1},P is incident light power, is wave length 490nm for blue LED and 647nm for red LED respectively.

The resulting photon flux expressed by (eq.(2)

$$J_{hv} = \frac{N_{hv}}{A \times N_A} \quad (2)$$

Wher A is area A of 7.85 10^{-2}cm^2, Nhv the number of photons per second , 1.38×10^{14}J/s for blue LED, NA, Avogadro's number=6.023×10^{23}

Results

SECM feedback mode

According to various applications, SECM has been a widely used tool to study interface dynamics[36,37]. SECM feedback mods, which use an ultra microelectrode (UME) to substrate and the resulting current response against the distance from the surface, can be used to access photochemical kinetics in solar cell sensitized[38-41]. Various studies indicate that after the dye is reduced (D⁻), illuminated dye excited (D*) creates a hole in the NiO semiconductor's valence band (VB). Eq. 3a-e describes a few photochemical reaction mechanisms in P-type DSSC[42,43]. Sensitized electrode-electrolyte interface photochemical reaction. Therefore, at the illuminated D-sensitized NiO electrode-electrolyte-UME probe[44,45]:

$$NiO/D + hv \rightarrow D^* /NiO : excitation \, (3a)$$

$$D^* /NiO \rightarrow D^- \rightarrow h^+ /NiO : charge\ separation \, (3b)$$

$$NiO(h^+) + D^- \longrightarrow NiO/D : germinate\ recombination \, (3c)$$

$$NiO(h^+)/D^- + I_3^- \rightarrow D/\ NiO\,(+) + I_2 + I^- : regeneration \, (3d)$$

$$3I^- - 2e^- \rightarrow I_3^- : regeneration\ on\ UME \, (3e)$$

When excited dye is exposed to light, it undergoes a charge separation, a hole injection into the valence band of NiO and dye reduction. The dye will then recombine with oxidized species of the electrolyte I_3^- and return to its ground state.

The model for this charge separation under illumination is (eq.3b) heterogeneous electron transfer (regeneration) I_3^-/D^- (eq.3d).Scanning probe in feedback mode, which is based on ultra-microelectrode movement near the surface of a conductive or non-conductive substrate and is defined by tip current for charge transfer reactions. The ultramicroelectrode (UME) probe functions as both an actuator and a sensor in this operating mode, responding to local changes in electrochemical activity while using feedback control to maintain a constant tip-sample distance.

The UME in the electrolyte solution determines the steady-state limiting current and the diffusion-limited reaction, which are given in (eq.4) and (eq.5), respectively.

$$O + ne^{-} \rightarrow R \ (4)$$

$$I_{T,\infty} = 4\pi F \left(\frac{k_{eff}}{k}\right) C\, r_T^2 \ (5)$$

Where, F: Faraday's constant, n is number of electrons transferred in reaction (eq. 4), k_{eff} reaction rate constant,C is concentration of electrolyte,r_T is UME radius and κ, normalized rate constant.

The photochemical kinetics of blue and red light of various wavelengths were studied in dye-sensitized NiO film. The impact of light intensity on the photochemical kinetics was examined by observing approach curves at different photon flux J_{hv}; as can be seen in ***(*Figures 3a and 3b)**, its value also increases with the increase in J_{hv}. When UME is close to the sample surface, tip current is modified by photo electrochemical interaction at the NiO/dye electrolyte interface **(Table 1)**.

Table 1: Normalized rate constants keff of CW1/NiO and C343/NiO in blue illumination D = 1.86 10^{-5} $cm^2 \cdot s{-1}$, rT = 12.5 µm

$J_{hv}/10^{-9}$ mol·cm^{-2} ·s^{-1}	Curve #	k	$k_{eff/}$10−3 cm·s−1
(a) CW1			
22.4	7	0.219	8.18
19.8	6	0.214	7.67
13.9	5	0.189	6.25
11.8	4	0.178	5.62
6.8	3	0.156	3.79
6.1	2	0.132	3.48
2.2	1	0.067	1.45
(b) C343			
22.4	7	0.213	4.93
19.8	6	0.205	4.64
13.9	5	0.185	3.82
11.8	4	0.174	3.46
6.8	3	0.137	2.37
6.1	2	0.129	2.18
2.2	1	0.065	0.92

The SECM feedback mode technique was used to examine the photo electrochemical reaction's kinetics by the electrolyte on NiO films with two dyes (C343 and CW1) of different intensities, as presented in Tables 1 and 2. The normalized experimental method curves at UME under blue LED light illumination for CW1/NiO are presented in Figure3(a).

Under blue LED light, the photon flux ranged from 2.210^{-9}mol. cm^{-2}.s^{-1} to 22.4 ×10^{-9}mol.cm^{-2}.s^{-1}. In blue LED for CW1/ NiO, the k_{eff} rate constant rose from 1.45×10^{-3} to 8.18×10^{-3}cm.s^{-1}. Figure 3(b) illustrates the normalized experimental approach curves at NiO/C343 under blue LED light at various intensities. As given in Table 1, NiO/C343 keff rate constant in blue LED rose from 0.9210^{-3} to 4.9310^{-3}cm.s^{-1}.

Figure 4(a) shows the experimentally normalized approach curves on C343/ NiO under red illumination flux density range d between 2. 12×10^{-9}mol.cm^{-2}s^{-1} to 14.7×10^{-9} mol. cm^{-2}.s^{-1} its rate constant k_{eff} ranged between 2.43×10^{-3} to 7.39×10^{-3} cm.s$^{-1.}$ Figure4(b) shows the approach curve on NiO/CW1 under red illumination at different intensities rate constant r anged between 1. 82×10−3 to 5.64×10^{-3}cm.s^{-1} in red LED as presented in **(Table 2)**.

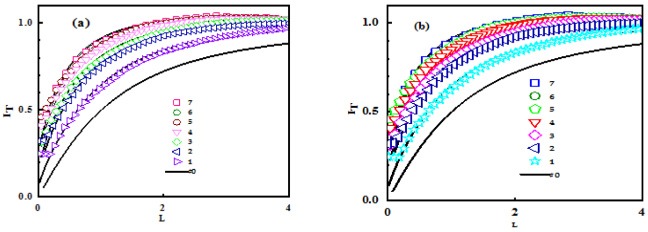

Figure 3: Normalized SECM feedback approach curves of a Pt disk UME towards (a) NiO/CW1, (b) NiO/C343 , under illumination by a blue LED. Photon flux density of LED in 10^{-9} mol cm-^{2} s-^{1}

The apparent heterogeneous rate constant k_{eff} for the photochemical reaction of the photo-reduced dye by I^{-} is obtained from $(k_{eff} = \kappa D/r_T)$with the diffusion coefficient of I^{-} in acetonitrile of 1.867×10^{-5}cm^2 s^{-1} and r_T of the particular UME used. The results are summarized in Table 1 for blue illumination, table 2 for red illumination respectively.

Fig. 5. is the k_{eff} vs J_{hv} plot for CW1 and C343 sensitized (a) blue light and (b) red light. An experiment value of k_{red} = 6.95×105 mol^{-1} . cm3 .s $^{-1}$ and Φhv(λ) = 3.16× 10^6 cm^2. mol^{-1} for the C343 blue, LED respectively. An experiment of kred = 7.95×10^5 mol^{-1}. cm^3 .s $^{-1}$ and Φhv(λ) = 3.32×10^6 cm^2. mol^{-1} for CW1 in the blue, LED, respectively Table 3. Upon back-illumination of the sensitized NiO film, the ground state dye is designated as D, photo-reduced dyes D^{-} and photo excited dye molecules D*.

Table 2: Normalized rate constants k_{eff} of C343/NiO and CW1/NiO in red illumination D = 1.86 10^{-5} cm^2 ·s^{-1} , r_T = 12.5 µm

$J_{hv}/10^{-9}$ mol·cm^{-2} ·s^{-1}	Curve #	k	$k_{eff/}10^{-3}$ cm·s^{-1}
(a) CW1			
14.7	7	0.048	7.39
13.1	6	0.046	7.09
12.1	5	0.044	6.89
9.4	4	0.041	6.21
6.8	3	0.034	5.31
4.2	2	0.027	4.01
2.12	1	0.016	2.43
(b) C343			
14.7	7	0.037	5.64
13.1	6	0.036	5.41
12.1	5	0.035	5.24
9.4	4	0.032	4.72
6.8	3	0.137	4.02
4.2	2	0.027	3.01
2.12	1	0.023	1.82

The mathematical expression for excited dye D* can be derived from mass conservation and steady-state approximations for photo excited dye surface concentrations given by eq.uation (eq.6) and reduced dye (eq.7).

$$\frac{\partial \Gamma_D^*}{\partial t} = J_{hv}\Phi_{hv} - k_{inj}\Gamma_D^* \quad (6)$$

$$\frac{\partial \Gamma_D^-}{\partial t} = k_{red}\Gamma_{D^-}[I_3^-]_s^{1/2} + k_{inj}\Gamma_D^* \quad (7)$$

Therefore, (eq.8) gives the rate constants of k_{red} for reduction of the reduced dye upon injection of the hole into the valance band of the NiO semiconductor by the reduced state of redox in the incident light upon it. A kinetic analysis rate constant k_{eff}, on the basis of reduction rate constant kred,dye absorption cross-section Φhv, sample thickness L, dye concentration Do and electrolyte concentration [] as

$$\frac{1}{k_{red}} = \frac{2L}{D^o}\left[\frac{I^-}{J_{hv}\Phi_{hv}} + \frac{1}{k_{eff}}\right] \quad (8)$$

Where , k_{eff} represents the regeneration rate **(Figures 4-6)** **(Table 3)**.

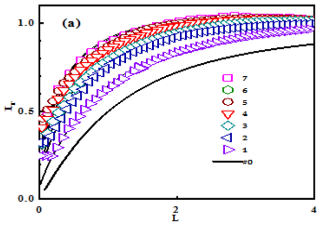

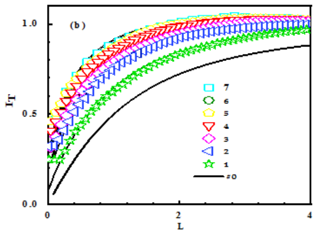

Figure 4: Normalized feedback approach curves for the approach of a Pt disk UME towards (a) NiO/C343, (b) NiO/CW1 in red Illumination

Table 3: Regeneration parameters for C343/NiO and CW1/NiO in blue illumination.

Dye	k_{red}/mol^{-1}cm^{3}s^{-1}	Φ_{hv}/cm^{2}mol^{-1}			Ep(eV)
CW1	$9.62\ 10^6$	$7.95\ 10^5$	-4.35	-2.8	-3.81
C343	$3.06\ 10^5$	$3.32\ 10^5$	-4.34	-0.92	-3.8

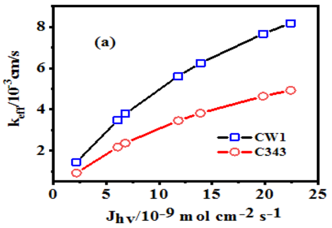

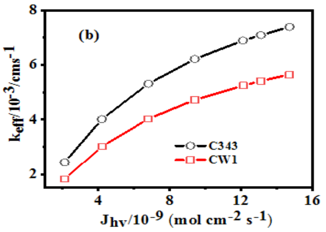

Figure 5: k_{eff} vs $J_{h\nu}$ for (a) CW1 and (b) C343 sensitized NiO films in blue and red LED.

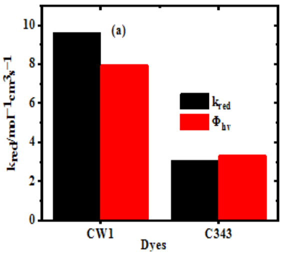

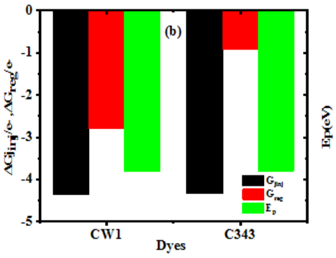

Figure 6: $k_{red\ hv}$, dye, the hole injection, the regeneration reaction and, the reduction potential of dyes

Figure 6a. Show that CW1 dye’s reduction rate constant, kred and absorption cross-section Φhv are much larger than C343 dye. Dye difference effect, which results from the shift of conduction band edge of p-type semiconductor (NiO), affects rate and direction of photochemical reaction drivers such as free energies of hole injection ΔG_{inj} per electron(eq.9), dye regeneration reaction, ΔG_{reg}(eq.11), per electron and excited state dye reduction potential Ep (eq.11) as shown in figure.6b.

$$\frac{\Delta G j_{inj}}{e^-} = [\mathrm{EV_{NiO}} - (\mathrm{E_{00}(D)^*} + \mathrm{E(D/D^-)})] \quad (9)$$

$$\frac{\Delta G_{reg}}{e^-} = [(I^-/I_3^-) - E(D/D^-)] \quad (10)$$

$$E_p(eV) = E_{00}(D*) + E(D/D-) \quad (11)$$

Where e is the elementary charge, E_{VB}: is the valence band potential of the NiO[45-47]. E_{00}(D*) is the energy of the excited dye, E(D/D-) is the reduction potential of the dye and E() is the reduction potential of the redox electrolyte (-0.28eV) in acetonitrile solvent and Ep is reduction potential of the excited state of the dye. From various studies, the valence band potential (EVB) of NiO is 0.54 V vs NHE[47-49], the E00 (D*) of C343 (-2.6eV) and CW1 (-0.693eV). The reduced state dye energy, (E(D/D-), for CW1 and(-3.12eV) and for C343 (-1.2eV)[50]. Using (eq.9), the free energy for hole injection (ΔG_{inj}) per electron is calculated to be (-4.35eV) and (-4.34eV) for both CW1 and C343 respectively.

In addition, the dye regeneration reaction per unit elementary charge for CW1 and C343 was -2.84eV and -0.29eV, respectively; the photochemical reaction between the dye and electrolyte must be feasible so that the two dyes’ reduction potential is more negative than the electrolyte’s (ΔGreg<0); for CW1 dye, a significantly higher free energy per charge and a slightly higher injection per electron were found, which would lead to a faster regeneration process than that of C343[48-50]. In other words, as shown by (Eq.11), the valence band edge of NiO is lower than the reduction potential of the dye’s excited state, which for CW1 and C343 is -3.81eV for CW1 and -3.8eV for C343. The aforementioned highlights the crucial finding that dye types have a significant impact on the photochemical parameters.

SECM measurement of different film thickness

Systematic research on the effect of film thickness on the photochemical kinetics of dye is lacking. Several investigations have been conducted on the film thickness of the macroscopic nature of dye sensitized solar cells parameters such as Voc, Jsc **(Figure 7)** and FF but not on the reaction rate and rate of dye photochemical kinetics at individual samples[46-49]. The film thickness has an indirect influence on the performance of dye sensitized solar cells, photochemical reaction and the possibility of dye assembly and therefore promoting more light absorption[19,20]. SECM feedback measurement allowed the examination of dye photochemical kinetics in a microscopic sample (Table 4).

This work studied six samples of thickness 2.8µm, 34µm, 3.8µm, 4.4µm, 5.4µm and 5.8µm. Figure 7(a) demonstrates the absorption spectra of C343 adsorbed at various thicknesses on porous NiO films. The spectra distinctly show broad bands of absorption having a peak near 490 nm, overlapped onto an background signal from scattering of light by the nickel oxide film **(Table 5)**. This confirms the successful pore dye saturation of the films for all films. The film thickness follows the trend of peak heights in the solid-state absorption on the surface NiO spectra, pick highest for 5.8µm (figure 6(a).(b) and lowest spectra pick for 2.8µm (figure 7(a)(g).

Table 4: Normalized rate constants k_{eff} of C343/NiO for different film thickness in blue illumination, $J_{hv}/10^{-9}$ mol·cm^{-2} ·s^{-1}, $k_{eff}/10^{-3}$ cms^{-1} S/

$J_{hv}/10^{-9}$	k_{eff}/ S28	k_{eff}/ S34	k_{eff}/ S38	k_{eff}/ S44	k_{eff}/ S54	k_{eff}/ S58
22.4	7.65	8.57	8.74	8.88	9.18	10.17
19.8	7.19	8.18	8.39	8.62	8.95	9.87
13.9	6.21	7.19	7.37	7.43	7.97	8.98
11.8	5.43	6.24	6.71	6.86	7.56	8.28
6.12	3.82	4.32	5.05	5.28	5.68	6.37
2.21	1.74	1.83	1.98	2.09	2.36	3.89

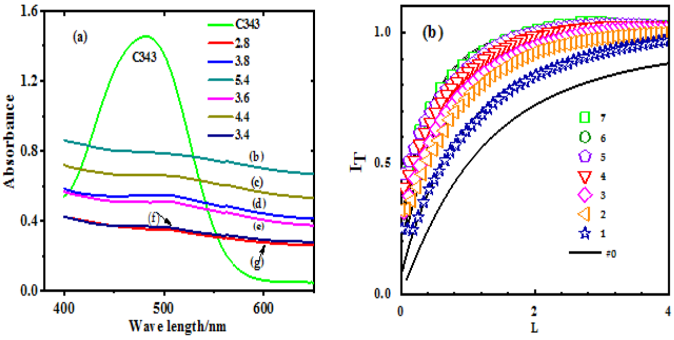

Figure 7: (a) Optical absorption spectra of NiO/C343 films of different thickness,(b) SECM approach curves obtained with Pt UME (rT = 12.5 mm) on C343-NiO films of thikness 28.

Table 5: Regeneration parameters Φhv and $k_{red,}$ of C343 by I- for different film thickness. Φhv/10^{6} (cm^{2}mol^{-1}), $k_{red}/10^{5}$ (mol^{-1}cm3 • s^{-1}) and mol cm^{-2}

L/10^{-6}m	$\Phi_{hv}/10^{6}$ (cm^{2}mol^{-1})	$k_{red}/10^{5}$ (mol^{-1}cm^{3}s^{-1})	$T_D/10^{-10}$mol cm^{-2}	$k_{reg/10-}$
28	3.71	5.65	5.15	0.188
34	3.89	5.46	5.79	0.171
38	4.28	4.98	6.02	0.162
44	4.98	4.55	7.27	0.151
54	5.27	3.95	8.32	0.136
58	5.58	3.88	9.31	0.131

Figure 7(b) are the normalized SECM approach curves recorded using Pt UME rT = 12.5µm coming towards C343/NiO films of 28µm thickness under illumination with different photon flux density. By changing the photon flux density J_{hv} of the blue illumination from 2.21×10^{-9}mol.cm^{-2}.s^{-1} to 22.4×10^{-9}mol.cm^{-2}.s^{-1}, keff changed from 1.74×10^{-3}cms^{-1} to 7.6×10^{-3}cms^{-1}for thickness of the sample 28µm **(Table 4)**. Such trend the value of keff at illuminated C343/NiO film, increases with the increase in Jhv. Normalized approach curves of other samples were recorded in supporting information. It can be seen that for same variation of photon flux density, the keff increased from lower to higher flux density in all the samples **(Figure 8)**.

For Diffusion-Controlled system Regeneration rate have invers reltion with film thkness

$$k_{reg} = \frac{1}{\sqrt{L}} \qquad (12)$$

By using equ.(12) in equ.(8)

$$k_{reg} = \sqrt{\frac{k_{red}}{D^{o}}\left[\frac{I^{-}}{J_{hv}\Phi_{hv}} + \frac{1}{k_{eff}}\right]} \quad (13)$$

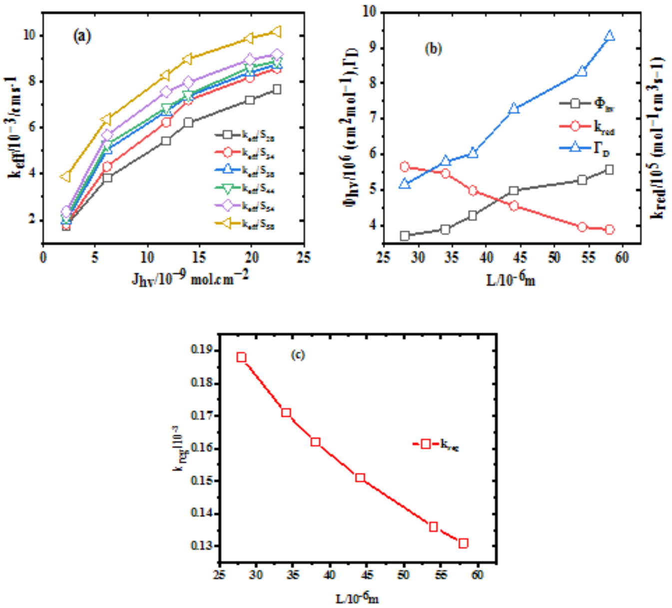

Figure 8: (a)$_{keff}$ vs. Jhv for six different C343/NiO photoelectrodes with systematically varied thickness; (b) k_{red}, $\Phi_{hv\ Dm}$ vs L/nm Thickness of film (c). Regeneration rate vs. Film thickness.

For all samples , the increased flux regeneration rate constant increased more than tripled relative to low flux density blue illumination regeneration rate constant. Above all, the dependence of regeneration rate constant k_{eff} , on dependence of sample thickness was shown evidently that the sample thickness is fairly meaningful to effective photochemical reaction.

The relationship between keff and Jhv is shown in Figure 8(a) for six different C343/NiO photo electrode samples with systematically different thicknesses. The relationship between sample thickness Lvs k_{red}, Φhv and Γ_D for six different samples is displayed in Figure 8(b). The increased dye deposition, which provides more opportunities for light absorption as film thickness increases, is the cause of the sample's increasing thickness. The constant of regeneration falls with increasing film thickness because the dye concentration on the NiO film surface increases and the photochemical reaction rate on the NiO/C343 surface is higher than that of the UME photochemical reaction. In the P-type DSSC, the situation is much more complex, though it is still possible to reach the same conclusion.

For electrodes from our set, the second major parameter, Φhv, was obtained as a function of film thickness. Due to the very slight spectral broadening that was observed when C343 adsorbed onto NiO, this is in fact expected to be a function of the dye's extinction coefficient, Φhv, which can at best be regarded as variable even at high concentrations of C343.

The quantity serves as a benchmark for the quantity of dye molecules per internal surface area.$Dc=\Gamma_D/(P.l)=\Gamma_D/(A.l)$ where the projected area of the SECM probe is DC dye concentration Γ_D NiO film surface dye content (mol cm^{-2}), p porosity (%), Lp(μm) and thickness of NiO film as shown Figure 8b. This makes sense because it is implicitly assumed that the sample size(NiO) varies for all films associated with the mean effects of the dye molecules on the surface. Higher concentrations of C343 molecules improve kred, which means that hole conduction in adsorbed dye C343 facilitates the regeneration of oxidized dye molecules.The absorption spectra's peak height tendency and the ΓD's tendency against film thickness are appropriate.The inverse relationship between film thickness and regeneration rate is depicted in Figure 8c. If diffusion or charge transport are limiting factors, thinner films typically promote faster regeneration and thiker film exihbet slow regeneration .

Conclusions

The photochemical kinetics of C343-sensitized NiO photo electrodes were investigated on a range of film thicknesses and it was discovered that the absorption cross section area Φ_{hv} and the rate constants kred were significantly different for the photo electrodes of systematically varied NiO thickness. The clear difference of regeneration parameters was analyzed for CW1/NiO and C343/NiO and both dyes' regeneration parameters showed significant variation in different wave lengths of illumination. The SECM kinetic model demonstrates significant variation in C343 photochemical kinetics constants k_{red} and absorption cross section Φ_{hv} for C343–NiO electrodes of systematically varied film thickness. It is concluded that the photochemical kinetics of the dye molecules and hole injection have been greatly impacted by the thickness of film and dye types in the present system. These findings highlight the critical role of film thicknesses in designing efficient dye-sensitized photocathodes for solar energy conversion, where modified thickness can exploit interfacial kinetics without compromising charge collection.

References

1. Bertoncello P, et al. Advanced Electrolyte Formulations for High-Efficiency Dye-Sensitized Solar Cells. Chemical Reviews 2023;123(8):4567-4592.
2. Chen X, et al. Hierarchical TiO_2 Nanostructures for Enhanced Charge Collection in DSSCs. Advanced Energy Materials 2022;12(34):2201234.
3. Fornazero J, et al. Plasmonic Gold Nanoparticles for Enhanced Light Harvesting in DSSCs. ACS Nano 2023;17(5):4985-4999.
4. Kim H, et al. Solid-State DSSCs with 14.2% Efficiency Using a CuSCN Hole Transporter. Nature Energy 2023;8(5):512-525.
5. Li Y, et al. Machine Learning-Assisted Discovery of Organic Dyes for DSSCs. Energy, Environ Sci 2023;16(4):1452-1465.
6. Park S, et al. Single-Atom Catalysts on TiO_2 for Reduced Charge Recombination in DSSCs. Nano Letters 2023;23(6):2345-2356.
7. Tefashe UM, et al. In Situ Spectro electro chemistry of Dye Regeneration Kinetics in DSSCs. J American Chem Society 2022;144(32):14567-14579.
8. Wang L, et al. Flexible DSSCs with Graphene-Based Counter Electrodes. Advanced Materials 2022;34(18);2106789.
9. Wu K, et al. Triple-Cation Perovskite-Sensitized DSSCs with 16.8% Efficiency. Sci Advances 2023;9(15):4560.
10. Zhang R, et al. Ultralow Recombination in DSSCs via Molecular Engineering of Dye-TiO_2 Anchoring. Nature Communications 2023;14:2345.
11. Zhao W, et al. Next-Generation Redox Shuttles for DSSCs: From Molecular Design to Device Integration. Chemical Society Reviews 2023;52(10):3567-3589.
12. Gibson EA, Plux LL, Fortage J, et al. Role of the Triiodide/Iodide Redox Couple in Dye Regeneration in p-Type Dye-Sensitized Solar Cells. Lagmuir 2012;28:6485-6493.
13. Wang ZY, Wang L, Zhang Y, Guo JN, Li H, Yan Y. Dye-Sensitized Solar Cells Based on Cobalt Containing Room Temperature Ionic, Liquid Redox Shuttles. RSC Advances 2017;7:13689-13695.
14. Odobel F, Pleux L, Pellegrin Y, Blart L. New Photovoltaic Devices Based on the Sensitization of p-Type Semiconductors: Challenges and Opportunities. Accounts of Chem Res 2010;43:1063-1071.
15. Nattestad A, Ferguson M, Kerr R, Cheng YB, Bach U. Dye-Sensitized Nickel(II) Oxide Photocathodes for Tandem Solar Cell Applications. Nanotechnology 2008;19:295304.
16. Fernando CAN, Kitagawa A, Suzuki M, Takahashi K, Komura T. Photoelectrochemical Properties of Rhodamine-C18 Sensitized p-CuSCN Photoelectrochemical Cell (PEC). Solar Energy Materials, Solar Cells 1994;33:301-315.
17. Yu M, Natu G, Ji ZQ, Wu Y. p-Type Dye-Sensitized Solar Cells Based on Delafossite CuGaO2Nanoplates with Saturation Photovoltages Exceeding 460 mV. J Physical Chemistry Letters 2012;3:1074-1078.
18. Euser TG, Harding PJ, Vos WL. Broadband Sensitive Pump-Probe Setup for Ultrafast Optical Switching of Photonic Nanostructures and Semiconductors. Review of Scientific Instruments 2009;80:073104.
19. Nechay BA, Siegner U, Achermann M, Bielefeldt H, Keller U. Femtosecond Pump-Probe Near-Field Optical Microscopy. Review of Scientific Instruments 1999;70:2758
20. Azima A, Düsterer S, Radcliffe P, et al. Time Resolved Pump-Probe Experiments beyond the Jitter Limitations at FLASH. Applied Physics Letters 2009;94:144102.
21. Xiong D, Xu Z, Zeng XW, et al. Hydrothermal Synthesis of Ultrasmall CuCrO2 Nanocrystal Alternatives to NiO Nanoparticles in Efficient p-Type Dye-Sensitized Solar Cells. Materials Chemistry 2012;22:24760-24768.
22. Cui J, Li PF, Chen ZF, et al. Phosphor Coated NiO-Based Planar Inverted Organometallic Halide Perovskite Solar Cells with Enhanced Efficiency and Stability. Applied Physics Letters 2016;109:171103.
23. Keis K, Magnusson E, Lindstrom H, Lindquist SE, Hagfeldt A. A 5% Efficient Photo Electrochemical Solar Cell Based on Nanostructured ZnO Electrodes. Solar Energy Materials and Solar Cells 2002;73:51-58.
24. Ito S, Zakeeruddin SM, Humphry-Baker R, et al. High-Efficiency Organic-Dye-Sensitized Solar Cells Controlled by Nanocrystalline-TiO2 Electrode Thickness. Advanced Materials 2006;18:1202-1205.
25. Martini LA, Moore GF, Milot RL, et al. Modular Assembly of High Potential Zinc Porphyrin Photosensitizers Attached to TiO2 with a Series of Anchoring Groups. J Physical Chemistry C 2013;117:14526-14533.
26. Turner GM, Beard MC, Schmuttenmaer CA. Carrier Localization and Cooling in Dye-Sensitized Nanocrystalline Titanium Dioxide. J Physical Chemistry B 2002;106:11716.
27. Heimer T, Heilweil EJ. Electron Injection, Recombination and Halide Oxidation Dynamics at Dye-Sensitized Metal Oxide Interfaces. J Physical Chemistry A 2000;104:4256.

28. Kuciauskas D, Mont JE, Villahermosa R, Gray HB, Lewis NS, McCusker JK. Transient Absorption Spectroscopy of Ruthenium and Osmium Polypyridyl Complexes Adsorbed onto Nanocrystalline TiO2 Photoelectrodes. J Physical Chemistry B 2002;106:9347.

29. Zhao C, Wittstock G. Scanning Electrochemical Microscopy of Quino-protein Glucose Dehyd Rogenase. Analytical Chem 2004;76:3145-3154.

30. Tefashe UM, Nonomura K, Vlachopoulos N, Hagfeldt A, Wittstock G. Effect of Cation on Dye Regeneration Kinetics of N719-Sensitized TiO2 Films in Acetonitrile-Based and Ionic-Liquid-Based Electrolytes Investigated by Scanning Electrochemical Microscopy. J Physical Chemistry C 2012;116:4316-4323.

31. Tefashe UM, Rudolph M, Miura H, Wittstock DS. Photovoltaic characteristics and Dye Regeneration Kinetics in D149-Sensitized ZnO with Varied Dye Loading and Film Thickness. Physical Chemistry Chemical Physics 2010:7533-7542.

32. Shen Y, Nonomura K, Schlettwein D, Zhao C, Wittstock G. Photoelectrochemical kinetics of Eosin Y-sensitized zinc oxide films investigated by scanning electrochemical Microscopy. Chemistry: A European J 2006;12:5832-5839.

33. Shen Y, Tinashe UM, Nonomurab K, Loewenstein T, Schlettwein D and Witt stock. G-Photoelectrochemical Kinetics of Eosin Y-Sensitized Zinc Oxide Films Investigated by Scanning Electrochemical Microscopy under Illumination with Different LED. Electrochimica Acta 2009;55:458-464.

34. Yazigi JA Jr, Anauate Nicolao F, Archetti Netto N. Magnetic resonance imaging reproducibility for rotator cuff partial tears in patients up to 60 years. BMC Musculoskelet Disord 2019;20:383-388.

35. Moore Y, Shotton E, Brown R, et al. Effects of incentive spirometry on perceived dyspnea in patients hospitalized with pneumonia. Med Surg Nursing 2018;27(1):19-23

36. Laver KE, Adey-Wakeling Z, Crotty M, Lannin NA, George S, Sherrington C. Telerehabilitation services for stroke. Cochrane Database of Syst Rev 2020;(1):010255.

37. Alemu AG, Alemu T. Dye Regeneration Kinetics of Sensitized Nickel Oxide Films under Illumination Investigated by Scanning Electrochemical Microscopy. Advances in Materials Physics, Chemistry 2021;11:78-92.

38. Zhang X, Leddy J, Bard AJ. Dependence of Rate Constants of Heterogeneous Electron Transfer Reactions on Viscosity. J American Chemical Society 1985;107:3719-3721.

39. Zhang X, Leddy J, Bard AJ. Dependence of Rate Constants of Heterogeneous Electron Transfer Reactions on Viscosity. J American Chemical Society 1985;107:3719-3721.

40. Cornut R, Lefrou C. New Analytical Approximation of Feedback Approach Curves with a Micro Disk SECM Tip and Irreversible Kinetic Reaction at the Substrate. J Electroanalytical Chem 2008;621:178-184.

41. Mirabel A, Barton SC. Numerical Correction of in Situ AFM-SECM Measurements. Analytical Chem 2021;93:12495-12503.

42. Wittstock G, Burchardt M, Pust SE, Shen Y, Zhao C. Scanning Electrochemical Microcopy for Direct Imaging of Reaction Rates. Angewandte Chemie Int Edition 2007;46:1584-1617

43. Tefashe UM, Loewenstein T, Miura H, Schlettwein D, Wittstock G. Scanning Electrochemical Microscope Studies of Dye Regeneration in Indoline (D149)-Sensitized ZnO Photoelectrochemical Cells. J Electroanalytical Chem 2010;650:24-30.

44. Adler D, Feinleib J. Electrical and optical properties of narrow-band materials. Phys Rev B 1970;2:3112.

45. Dare-Edwards MP, Goodenough JB, Hamnett A, Nicholson ND. Photo electrochemistry of nickel(II) oxide. J Chem Soc Faraday Trans 1981;77:643-661.

46. Adler D, Feinleib J. Electrical and optical properties of narrow-band materials. Phys Rev B 1970;2:3112-3134.

47. He J, Lindstro¨m H, Hagfeldt A, Lindquist SE. Dye-sensitized nanostructured tandem cell - first demonstrated cell with a dye-sensitized photocathode. Sol Energy Mater Sol Cells 2000;62:265-273.

48. Qin P, Linder M, Brinck T, Boschloo G, Hagfeldt A, Sun L. Adv Mater 2009;21:2993-2996.

49. Peng Q, Joanna W, Elizabeth A, et al. Synthesis and Mechanistic Studies of Organic Chromophores with Different Energy Levels for p-Type Dye-Sensitized Solar Cells. J Physical Chemistry C 2010;114:4738-4748.

50. Bard AJ, Denuault G, Friesner RA, Dornblaser BC, Tuckerman LS. Scanning electrochemical microscopy: theory and application of the transient (chronoamperometric) SECM response. Anal Chem 1991;63:1282.